

# Size-dependent effects of ZnO nanoparticles on the photocatalytic degradation of phenol in a water solution

E. Kusiak-Nejman<sup>a,\*</sup>, J. Wojnarowicz<sup>b</sup>, A.W. Morawski<sup>a</sup>, U. Narkiewicz<sup>a</sup>, K. Sobczak<sup>c</sup>, S. Gierlotka<sup>b</sup>, W. Lojkowski<sup>b</sup>

<sup>a</sup> Department of Inorganic Chemical Technology and Environment Engineering, Faculty of Chemical Technology and Engineering, West Pomeranian University of Technology in Szczecin, Pułaskiego 10, 70-322 Szczecin, Poland

<sup>b</sup> Institute of High Pressure Physics, Sokolowska 29/37, 01-142 Warsaw, Poland

<sup>c</sup> Faculty of Chemistry, Biological and Chemical Research Centre, University of Warsaw, Żwirki i Wigury 101, 02-089 Warsaw, Poland

## ARTICLE INFO

### Keywords:

Photocatalytic degradation  
Phenol  
ZnO nanoparticles (NPs)  
Microwave solvothermal synthesis (MSS)  
Recombination time

## ABSTRACT

The effect of the ZnO nanoparticles (NPs) size on the photocatalytic degradation of phenol in a water solution under the influence of UV and Vis radiation was discussed. For the first time, research on photocatalytic degradation has used ZnO NPs produced by only one method (microwave solvothermal synthesis without heat treatment or other processes of reduction/oxidisation of the surface of NPs samples). ZnO NPs average size was determined using the Scherrer's formula, Nanopowder XRD Processor Demo web application, by converting the results of the specific surface area-density, and TEM tests. The ZnO NPs (average size between 23 nm and 71 nm) characterise by uniform morphology and narrow size distribution. The photocatalytic performance of ZnO NPs increases with the increase of the particle size and the decrease of the specific surface area. For both UV and Vis radiation, the highest reaction rate for phenol degradation was found for ZnO sample with the average particle size of 71 nm. Low concentrations of resorcinol and hydroquinone (co-products of phenol degradation) were found for UV light photocatalytic test. However, high concentrations of hydro- and p-benzoquinone were observed for visible light photoactivity due to the slower decomposition of the main contamination associated with the utilized of other type of radiation. The photocatalytic activity was found to be attributable to the decrease in the charge carrier recombination rate.

## 1. Introduction

Nanomaterials are characterised by at least one dimension in the range of 1–100 nm and specific properties, different from those observed for their coarse-grained counterparts. All fundamental properties, like chemical, optical, mechanical, electrical, magnetic, are size-dependent [1,2]. Then, it is of particular importance to produce nanomaterials of well-controlled particle shape and size, as well as a narrow particle size distribution. The issue is especially crucial in the area of catalysis, where a chemical reaction occurs at the catalyst surface and with an increasing surface-to-volume ratio of atoms, the concentration of active sites exposed for the reactants adsorption and activation increases. Surface structure and electronic properties change dramatically at the nano- and sub-nano scale, which is extremely important for the catalytic performance. Despite the size of catalyst particles, the size of carrier particles can be important as well, as was demonstrated by Carretin et al. [3] for

the case of a gold catalyst supported on ceria and applied in CO oxidation. The activity of ceria with a particle size of 3.3 nm (specific surface area of 180 m<sup>2</sup>/g) was two orders of magnitude greater compared with a ceria material having an average particle size of 15.9 nm (specific surface area of 70 m<sup>2</sup>/g). The authors explained the phenomenon by a synergistic effect of nano-Au and nano-ceria, enhancing the formation of highly reactive oxygen species at one-electron defect sites of the support.

Nanotechnology enables nowadays not only to produce small catalyst particles but also to expose a preferred crystalline plane (the most active in a reaction), by assembling nanocatalyst particles from building nano-blocks. Then, thanks to nanotechnology, it is possible to extend the approach from “smaller – is better” to “optimum morphology is better”. For example, Hu et al. [4] carried out the combustion of methane over Co<sub>3</sub>O<sub>4</sub> nanosheets, nanobelts and nanocubes. The reaction rate was two times faster over the nanosheets than on the nanocubes. The methane combustion catalytic activity of crystal planes followed the order {112}

\* Corresponding author.

E-mail address: [ekusiak@zut.edu.pl](mailto:ekusiak@zut.edu.pl) (E. Kusiak-Nejman).

<https://doi.org/10.1016/j.apsusc.2020.148416>

Received 21 July 2020; Received in revised form 20 October 2020; Accepted 6 November 2020

Available online 12 November 2020

0169-4332/© 2020 Elsevier B.V. All rights reserved.

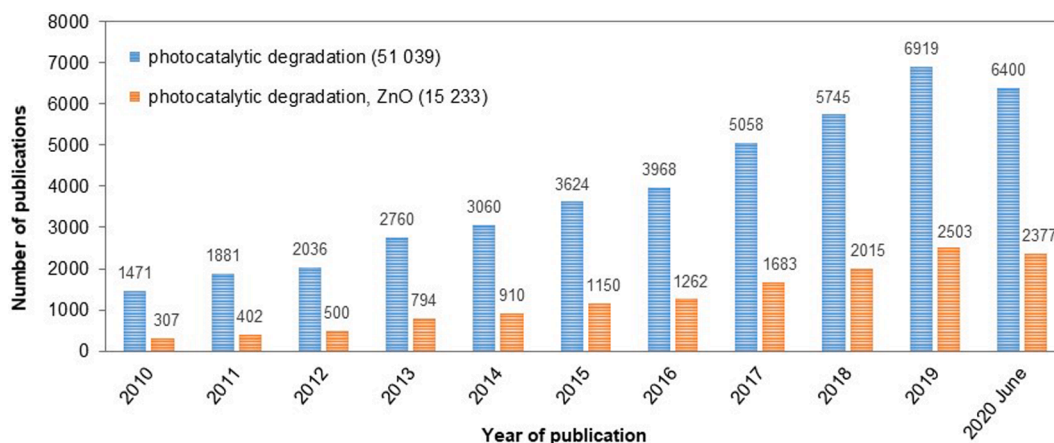


Fig. 1. The number of scientific publications referring to the search of “photocatalytic degradation” and “photocatalytic degradation, ZnO” phrases published in the period 2010–2020. Source: ScienceDirect (accessed June 29, 2020).

> {011} ≫ {001}.

Moreover, thanks to nanotechnology, it is now time to revise the rule “smaller is better” because it is not always the case. In the subnano regime, the precise number of atoms in a catalyst particle becomes important, and some optimum value can be determined, as was shown by Crompton et al. [5] for a structure-sensitive reaction of ethylene hydrogenation on the platinum catalyst, in the subnano particle size regime of Pt<sub>7</sub>–Pt<sub>40</sub>, with a maximum reactivity observed for Pt<sub>13</sub>.

The situation becomes more sophisticated in the case of photocatalysis when additional phenomena occur. In a photocatalytic process under the flux of photons, the electrons from the valence band are excited and transported to the conduction band, where a corresponding number of holes are created as well. Then, the group of photocatalysts is limited to semiconductors, with bandgap and band position enabling to utilise light energy effectively.

The charges generated in the conduction band, separate from each other and move to the active sites at the photocatalyst surface. Cophotocatalysts can also be applied, promoting the separation and migration of photogenerated charge carriers, lowering the activation barrier, favouring desired reaction selectivity and inhibiting the back-recombination reaction. The nanostructure is a positive feature not only providing a high specific surface area but also a direct pathway for electron transport, facilitating separation of photogenerated electron-hole pairs. The optimum nanoparticle size is determined as a result of a combination of specific surface area, charge-carrier-dynamics and light absorption efficiency [6].

Wang et al. [7] found an optimal size of titania nanoparticles (10 nm) as the most effective in the photocatalytic decomposition of chloroform. Zhang et al. [8] explained the existence of such an optimum through the competing effect of specific surface area and charge carrier recombination dynamics. On the other hand, a decrease in particle size increases the rate of surface charge recombination. When the particles are sufficiently small, the surface recombination can become prevailing, because the charge carriers are formed neighbouring surface, and the recombination process is faster than interfacial charge transfer [9].

Murakami et al. [10] determined an optimum of the photocatalytic activity for the particles of decahedral anatase as 40 nm when the controllable size of investigated particles varied from 25 to 60 nm. The authors explained the existence of the optimum as due to the balance between the efficient separation of redox sites and large specific surface area. Smaller titania particles (between 4.5 and 29 nm) were investigated by Koci et al. [11] in the process of photocatalytic reduction of carbon dioxide. The optimum was determined for the particle size of 14 nm, and the authors stated that it was due to competition of specific surface area, charge-carrier dynamics and light absorption efficiency.

The type of species deposited on the photocatalyst surface also can

cause a suppression of recombination or charge-carriers trapping, as it was shown for the case of the titania-graphene composite in the paper of Kusiak-Nejman et al. [12].

Surface modification of a photocatalyst with metals can cause a plasmonic resonance effect, generating “hot” electrons and enabling an enhancement of charge density and/or extension the light absorption spectrum to the visible region. It was proved mainly for noble metals (Zaleska et al. [13], Lee et al. [14], Du et al. [15], however, there are also reports about base metals, like Ni, Fe, Co [16] or Cu [17].

Photocatalytic degradation of organic water pollutants is a topic which is developing quite dynamically nowadays and might become the key technology of sewage treatment [18–20]. Such semiconductors as titanium dioxide (TiO<sub>2</sub>) [21,22], cadmium sulphide (CdS) [23] and zinc oxide (ZnO) [24–26] enjoy a particular interest on the part of research groups dealing with the issue of photocatalysis. Currently, scientists focus on the photocatalytic properties of ZnO because the band gap of this material (3.37 eV [27]) is similar to the band gap of TiO<sub>2</sub> (3.2 eV [28]). The growing popularity of ZnO in photocatalytic degradation applications could be confirmed by the search results of the phrases “photocatalytic degradation” (51 039 matches) and “photocatalytic degradation, ZnO” (15 233 matches) in the ScienceDirect scientific publication search engine (Fig. 1).

The methods of obtaining ZnO nanomaterials (ZnO NMs) which are reported in the literature most often are sol-gel [29–31], calcination [29,30], precipitation [29–32], hydrothermal synthesis [29,30], solvothermal synthesis [29,30], combustion synthesis [30,32], mechanochemical process [32], micro-emulsion synthesis [29,31,32], green synthesis [33–37], vapour techniques [30,38,39] and microwave radiation assisted syntheses [40,41]. Despite the fact that the publication of a considerable number of papers so far [40], the topic of repeatable syntheses and properties of ZnO NMs has still been quite controversial. Obtaining ZnO NPs with homogenous sizes and at the same time, homogeneous properties is a quite difficult task, which was discussed by us in the overview paper [40]. McLaren et al. [42] showed that the photocatalytic activity of ZnO NMs was strongly dependent on the size and shape of nanocrystals. Sun et al. described the influence of morphology on the photocatalytic activity of ZnO NMs [43]. Therefore, it is crucial to skilfully select the synthesis method and the preparation process of the ZnO NPs samples, because this makes it possible to avoid unrepeatable properties of ZnO NPs caused, e.g. by contamination or heterogeneity of the sample (size, shape). The appearance of new types of microwave reactors [44,45] permitted the development of unique synthesis methods [40], which make it possible to obtain homogeneous ZnO NPs with controlled properties and pharmaceutical purity.

Articles concerning photocatalytic degradation in the presence of ZnO already account for almost 28% of the number of all the scientific

papers referring to the topic of “photocatalytic degradation” (Fig. 1). The main topic in the majority of papers is research on the impact of the ZnO NPs synthesis method on the photocatalytic degradation properties [24,46–50], while ZnO NPs with various sizes are obtained by means of additional soaking of samples at high temperatures in various gaseous atmospheres (oxidising, reducing) [51–56]. Some authors also perform modifications of the surface of ZnO NMs by immersing them in reducing or oxidising solutions (e.g.  $\text{NaBH}_4$  [57]) [24]. There are also papers where the surface of ZnO NMs is modified with a polymer (e.g. polyaniline [58]) [24]. The majority of authors [24,46–56] did not provide the results of ZnO sample density in their papers. ZnO NPs density is the primary parameter which permits assessment of the quality of ZnO crystals used for the tests, e.g. in terms of the presence of an amorphous phase. The electron spin state and the structure of the surface of the ZnO NPs are assessed with the use of the electron paramagnetic resonance (EPR) spectroscopic technique [52,53], which is also often called electron spin resonance (ESR) spectroscopic technique.

One of the popular reference substances used for researching the suitability of photocatalysts is phenol [59]. The literature offers a range of publications discussing the photocatalytic degradation of phenol in the presence of ZnO catalysts [60–72]. The authors in their papers [60–68] described the influence of critical conditions of the process such as the photocatalyst quantity, the initial pH of the solution, the initial phenol concentration and the contact time on the reaction rate. Tao et al. [69] determined the products of photocatalytic degradation of phenol using ZnO NPs, which proved to be hydroquinone, catechol, benzoquinone, acetic acid, and proposed photocatalytic degradation pathways of phenol under the UV irradiation. Morales-Flores et al. [70] proved on the example of Pt-ZnO composite that by selecting the composition of the composite based on the ZnO matrix, it was possible to selectively control the type of product of the photodegradation of phenol. Udom et al. [71] presented an overall model for the variation in phenol degradation rate for the function of the intensity of UV light and pH level of the solution. For constant pH, Udom et al. [71] stated that the reaction rate was approximately linear and depending on the intensity of UV light, while for a constant intensity of UV light radiation the reaction rate assumed approximately the form of the third-order polynomial function in pH. Similar research concerning the reaction rate was performed by Ye et al. [72], who used the Langmuir–Hinshelwood model to analyse the kinetics of the photocatalytic degradation of phenol over ZnO nanosheets. Hu et al. [73] showed that ZnO with the average size of 500 nm ( $\text{SSA} = 3.7 \text{ m}^2/\text{g}$ ) displayed higher photocatalytic activity than ZnO with the average size of 50 nm ( $\text{SSA} = 12.4 \text{ m}^2/\text{g}$ ). The ZnO powder used by Hu et al. [73] was different, apart from the average particle size, in the method of production: ZnO 50 nm was produced by the chemical precipitation method, while 500 nm ZnO was produced by oxidation of the metal in oxygen. It is common knowledge that the photocatalytic activity of materials increases in line with the decrease in the particle size and simultaneously with the increase in the specific surface area [74,75]. The results obtained by Hu et al. [73] do not satisfy this principle, and the authors explained them with the decisive impact of the method of ZnO preparation on ZnO photocatalytic properties. Dodd et al. [9] produced nanoparticulate ZnO in the range of 28–57 nm by mechanical milling and measured hydroxyl radicals concentration as a function of irradiation time. The optimum of photocatalytic activity was determined for particles of 33 nm. The authors explained the existence of the optimum as an effect of the competition between charge carrier recombination rate and specific surface area. Li et al. [76] demonstrated in their paper that the photocatalytic activity of ZnO powder depended on the crystallinity rather than on the specific surface area value and also considerably on the type of ZnO NPs morphology. Parida et al. [77] suggested that the photocatalytic activity of ZnO depended on such parameters as surface area, surface acidity and method of ZnO production.

To contribute somehow to expanding the knowledge on photocatalysis of nanostructured materials, we applied a model reaction of

**Table 1**Results of the analysis of  $\text{H}_2\text{O}$  content in the precursors of ZnO NPs.

Sample	Actual $\text{H}_2\text{O}$ concentration, $C_{\text{H}_2\text{O}}$ (wt.%)
ZnO (1% $\text{H}_2\text{O}$ )	$1.03 \pm 0.01$
ZnO (2% $\text{H}_2\text{O}$ )	$2.02 \pm 0.02$
ZnO (3% $\text{H}_2\text{O}$ )	$3.03 \pm 0.02$
ZnO (4% $\text{H}_2\text{O}$ )	$3.02 \pm 0.03$
ZnO (5% $\text{H}_2\text{O}$ )	$5.04 \pm 0.06$
ZnO (6% $\text{H}_2\text{O}$ )	$6.05 \pm 0.04$

phenol decomposition to study the effect of nanoparticle size of ZnO on the reaction rate. Most publications indicate that the photocatalytic activity decreases with the increase of ZnO crystallites size. In this paper, we observed and explained for the first time entirely the opposite trend.

## 2. Materials and methods

### 2.1. Substrates and synthesis of ZnO NPs

The following chemicals were used as received: zinc acetate dihydrate ( $\text{Zn}(\text{CH}_3\text{COO})_2 \cdot 2\text{H}_2\text{O}$ , analytically pure, Avantor Performance Materials Poland S. A.); ethylene glycol (EG, ethane-1,2-diol,  $\text{C}_2\text{H}_4(\text{OH})_2$ , pure, Chempur, Piekary Śląskie, Poland); deionised water ( $\text{H}_2\text{O}$ ) (specific conductance  $< 0.1 \mu\text{S}/\text{cm}$ , HLP 20UV, Hydrolab, Straszyn, Poland).

The microwave solvothermal synthesis procedure, described in our previous papers [78–81], was used for obtaining ZnO NPs. The particle size was tuned through a controlled amount of water in the precursor ( $500 \text{ cm}^3$ ), which was obtained by dissolving zinc acetate ( $0.3037 \text{ mol}/\text{dm}^3$ ) in ethylene glycol.  $80 \text{ cm}^3$  was poured into six  $100 \text{ cm}^3$  sealed containers (PP) each and an analysis of the initial water content in the precursor solution was carried out: it amounted to  $1.03 \pm 0.01 \text{ wt}\%$ . Then such water quantities were calculated and added to the containers with the precursors that the following final water concentrations could be achieved 1–6 wt%. The results of the tests of actual final concentrations of  $\text{H}_2\text{O}$  in the obtained precursors are presented in Table 1.

The following microwave reactor was used for the syntheses: Model 02–02, ERTEC, Poland (600 W, 2.45 GHz), with the following setpoints: precursor volume poured into the reaction vessel:  $75 \text{ cm}^3$ ; reaction duration: 25 min; cooling duration: 20 min; the temperature of reaction chamber bottom:  $190 \text{ }^\circ\text{C}$ ; microwave power: 100%. The obtained suspensions were centrifuged, rinsed intensively with deionised water four times, and dried in the freeze dryer.

### 2.2. Characterisation methods

Detailed descriptions of the measurement procedures used for analysing the ZnO NPs samples are included in our earlier publications [78–81]. An automatic coulometric titrator with the integrated Karl Fischer method (Cou-Lo AquaMAX KF, GR Scientific, United Kingdom) [79,81] was used for analysing the  $\text{H}_2\text{O}$  content. The phase composition was determined by the X-ray diffraction method (XRD) (2 theta from  $28^\circ$  to  $72^\circ$ , room temperature,  $\text{CuK}\alpha 1$ , X’Pert PRO, Panalytical, the Netherlands). To determine the crystallite size, the Scherrer’s formula [78] and the FW15/45M method of XRD peak profile analysis [82–84] was used, which permitted also determining the crystallite size distribution. The morphology of NPs was determined using the scanning electron microscopy (SEM) (ZEISS, Ultra Plus, Germany).

The density of NPs samples was determined using the helium pycnometer at the temperature of  $24 \pm 1 \text{ }^\circ\text{C}$  (ISO 12154:2014, AccuPyc II 1340 FoamPyc V1.06, Micromeritics, USA). The specific surface area of NPs was determined by analysing the nitrogen adsorption isotherm by the Brunauer-Emmett-Teller (BET) method (ISO 9277:2010, Gemini 2360, V 2.01, Micromeritics) at the P/P0 range of 0.05–0.25 using multipoint BET equation. The average pore width was calculated by the

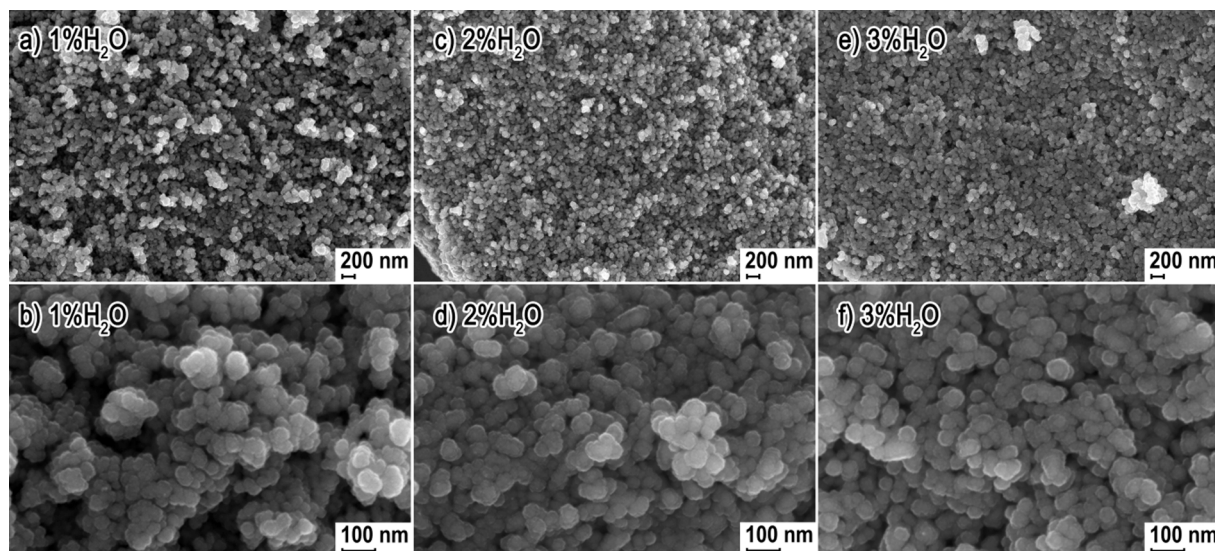


Fig. 2. SEM images of ZnO NPs obtained from precursors with varied H<sub>2</sub>O content: a) and b) 1%; c) and d) 2%; e) and f) 3%.

Barrett-Joyner-Halenda (BJH) method using adsorption isotherms at the  $p/p_0$  range of 0.001–0.99. The total pore volume of samples was estimated from the amount of adsorbed nitrogen at  $p/p_0 = 0.9896$ . The obtained data of the adsorption isotherms were analysed by us using the MicroActive software V4.03 (Interactive Data Analysis Software, Micromeritics). The obtained results of the specific surface area and density enabled calculating the average particle size with the assumption that all particles were spherical and identical [78]. The size distribution of NPs was determined by the bright field and the dark field technique for the analysis of microscopic images from the transmission electron microscopy (TEM) (Talos F200X, Thermo Scientific™, Waltham City, Massachusetts, MA, USA) based on the theoretical model assuming spherical particles with a log-normal size distribution [81].

The FT/IR-4200 spectrophotometer (Jasco Co., Tokyo, Japan) equipped with a diffuse reflectance accessory (PIKE Technologies, Madison, WI, USA) was used to characterise the structure of obtained ZnO nanoparticles photocatalysts. The FTIR/DR spectra were collected with  $4\text{ cm}^{-1}$  resolution in the range of wavenumber  $400\text{--}4000\text{ cm}^{-1}$ .

The photoelectric spectrometer (Instytut Fotonowy Sp. z o.o., Kraków, Poland) equipped with intensity-modulated photocurrent/

photovoltage module was utilised for measuring the minority carriers lifetime (positively charged holes in case of n-type semiconductor). Then the software options converted the obtained results into the recombination time of the ZnO minority carriers. Potassium chloride (pure p.a., Firma Chempur, Gliwice, Poland) solution with a concentration of 0.1 M was used as an electrolyte solution. A silver chloride electrode (Elmetron, Zabrze, Poland) was used as a reference electrode, a platinum wire as a counter electrode and indium thin oxide coated PET foil with the surface resistivity of  $60\ \Omega/\text{sq}$  (Merck KGaA, Darmstadt, Germany) covered with a thin film of the tested sample, was utilised as working electrode.

### 2.3. Photocatalytic activity tests

The photocatalytic activity of tested samples under UV and visible light irradiation was determined based on the oxidative decomposition of phenol (analytical grade  $\geq 99\%$ , Avantor Performance Materials Poland S.A., Gliwice, Poland). 20 mg of the appropriate photocatalyst (concentration of  $0.2\text{ g}/\text{dm}^3$ ) was suspended in  $100\text{ cm}^3$  of aqueous phenol solution with the initial concentration of  $10\text{ mg}/\text{dm}^3$ . Prior to the

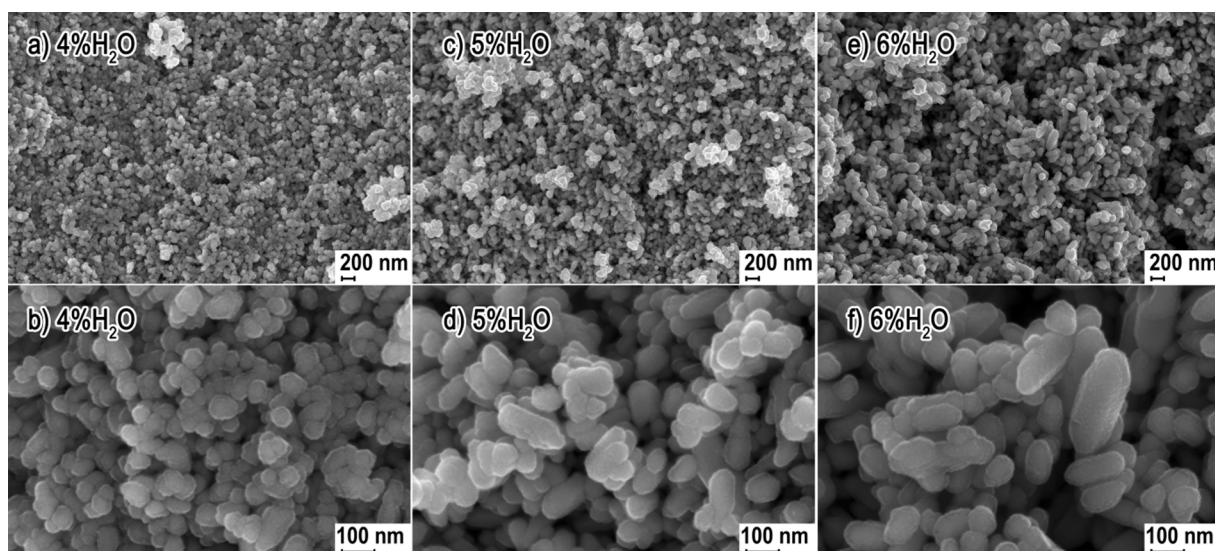


Fig. 3. SEM images of ZnO NPs obtained from precursors with varied H<sub>2</sub>O content: a) and b) 4%; c) and d) 5%; e) and f) 6%.

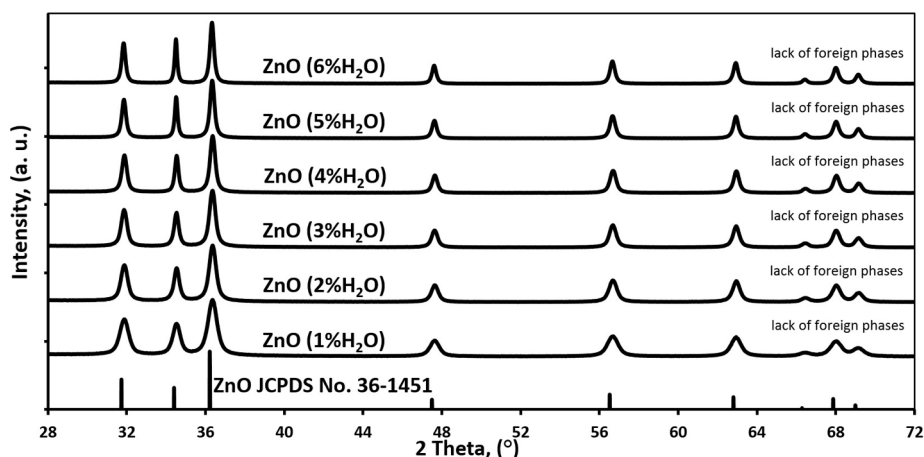


Fig. 4. X-ray diffraction patterns of ZnO NPs.

light exposition, the suspension was stirred (at 1000 rpm) for 30 min in the dark to ensure the establishment of the adsorption-desorption equilibrium. Next, the suspension was continuously radiated with the UV light source (6 lamps, 20 W each, 40 cm long, Koninklijke Philips N. V., Amsterdam, Netherlands), and Vis light source (20 lamps, 20 W each, 25 cm long, Koninklijke Philips N.V., Amsterdam, Netherlands) for 5 h. During the radiation, 5 cm<sup>3</sup> of phenol solution was taken every 30 min to observe the changes of phenol concentration, thus determine the photocatalytic activity of tested nanoparticles.

The temperature of the photooxidation reaction was kept at 25 °C using a thermostatic chamber. The radiation intensity of the utilised light source was 110 W/m<sup>2</sup> of UV and 5 W/m<sup>2</sup> of Vis (measured using the LB 901 radiation intensity meter with CM3 and PD204AB Cos sensors, LAB-EL Elektronika Laboratoryjna s.j., Reguly, Poland). The changes of concentration of phenol and its degradation derivatives (calibration curves prepared for benzoquinone, hydroquinone, catechol and rezoncine) were performed on HPLC Elite LaChrome chromatograph (Hitachi Ltd., Schaumburg, IL, USA), equipped with an auto-sampler, binary solvent delivery system and UV detector, was coupled to LiChroCART®250-4 Purospher®STAR RP-18 end-capped (5 µm) analytical column (Merck KGaA, Darmstadt, Germany). The mobile phase used was a mixture of methanol (HPLC grade, Scherlab S.L., Barcelona, Spain) and water (ultrapure water, Millipore Elix Advantage water purification system, Merck KGaA, Darmstadt, Germany with the conductivity of 0.05 µS/cm at 25 °C) in the volumetric proportion of 30:70, respectively. Tested samples of 100 µm<sup>3</sup> were injected in the analytical column.

### 3. Results and discussion

#### 3.1. Morphology

Figs. 2 and 3 present typical SEM images for the obtained ZnO NPs samples. Images 2a, 2c, 2e, 3a, 3c and 3e present a uniform morphology of ZnO NPs. Images 2b, 2d, 2f, 3b, 3d and 3f show the size of individual NPs and their uniform shape. SEM images (Figs. 2 and 3) reveal an impact of the change in H<sub>2</sub>O content in the precursor on the size of the obtained ZnO NPs and the shape change. We reported an identical observed effect of H<sub>2</sub>O on the changes to ZnO NPs properties in our previously published papers [78–81]. For the water content from 1% to 4% in the precursor, the average size of spherical ZnO NPs increases from circa 25–40 nm to 50–65 nm. For the water content of 5% and 6%, in turn, elliptical NPs are visible apart from spherical NPs. It can be concluded from the comparison of SEM images that the particle size distribution for the 5% H<sub>2</sub>O and 6% H<sub>2</sub>O samples must be considerably wider than the size distributions for samples with the water content from

Table 2  
Characteristics of ZnO NPs samples.

Sample	Specific surface area by gas adsorption, $a_s \pm \sigma$ (m <sup>2</sup> /g)	BJH adsorption average pore width (Å)	Total pore volume at $p/p_0 = 0.9896$ (cm <sup>3</sup> /g)	Skeleton density by gas pycnometry, $\rho_s \pm \sigma$ (g/cm <sup>3</sup> )
ZnO (1% H <sub>2</sub> O)	46.4	239.5	0.2893	5.24 ± 0.02
ZnO (2% H <sub>2</sub> O)	35.9	240.2	0.2575	5.31 ± 0.02
ZnO (3% H <sub>2</sub> O)	31.8	289.2	0.2505	5.42 ± 0.03
ZnO (4% H <sub>2</sub> O)	23.1	401.8	0.2310	5.46 ± 0.03
ZnO (5% H <sub>2</sub> O)	16.5	498.7	0.2128	5.49 ± 0.02
ZnO (6% H <sub>2</sub> O)	12.9	457.3	0.1444	5.51 ± 0.02

Table 3  
Comparison of the ZnO NPs size from different methods.

Sample	Average particle size from SSA BET, $d \pm \sigma$ (nm)	Average crystallite size from Nanopowder XRD Processor Demo, $d \pm \sigma$ (nm)	Average crystallite size, Scherrer's formula, based on XRD, $d_a, d_c$ (nm)	Average particles size from TEM, $d \pm SE$ (nm)
ZnO (1% H <sub>2</sub> O)	25	21 ± 5	19a, 17c	23 ± 1
ZnO (2% H <sub>2</sub> O)	32	29 ± 8	26a, 33c	27 ± 1
ZnO (3% H <sub>2</sub> O)	35	33 ± 9	31a, 39c	32 ± 1
ZnO (4% H <sub>2</sub> O)	48	40 ± 12	35a, 49c	44 ± 1
ZnO (5% H <sub>2</sub> O)	66	52 ± 19	41a, 61c	57 ± 2
ZnO (6% H <sub>2</sub> O)	85	58 ± 22	46a, 68c	71 ± 1

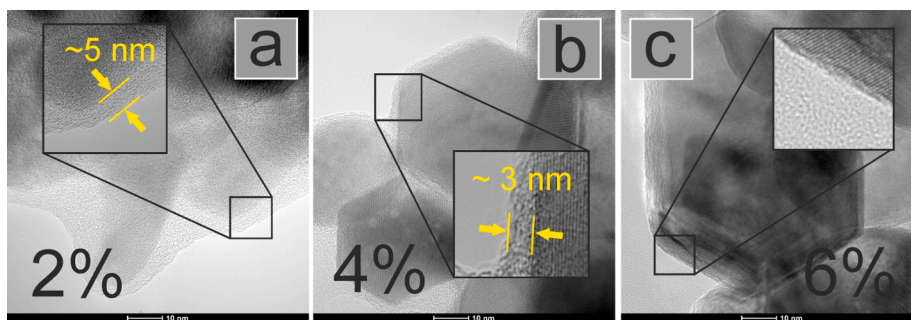


Fig. 5. TEM images of ZnO NPs obtained from precursors with varied H<sub>2</sub>O content: a) 2%; b) 4%) and f) 6%.

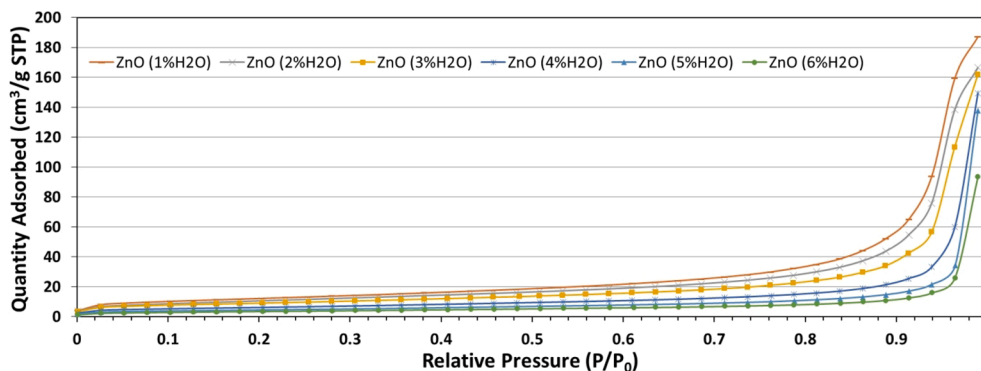


Fig. 6. Nitrogen adsorption isotherms of ZnO NPs. STP means standard temperature and pressure.

1% to 4%, which is caused by the presence of several particles exceeding 200 nm.

### 3.2. Phase composition

Fig. 4 presents the X-ray diffraction patterns of the synthesised ZnO NPs powders. At room temperature, the wurtzite hexagonal structure is the thermodynamically stable crystalline structure of ZnO [85]. All diffraction peaks visible in Fig. 4 were matched with the data of the reference sample of ZnO reported in PDF card No. 36-1451 [78], which

means that the obtained ZnO NPs samples were characterised by the wurtzite hexagonal structure. No presence of crystalline impurities was observed in the prepared ZnO NPs samples within the detection limit of the XRD method. Fig. 4 indicates a noticeable influence of the increase in the water content in the precursor on the narrowing of peak width for individual ZnO NPs samples, which means an increase in ZnO NPs crystallite size in line with the increase in the H<sub>2</sub>O content in the precursor.

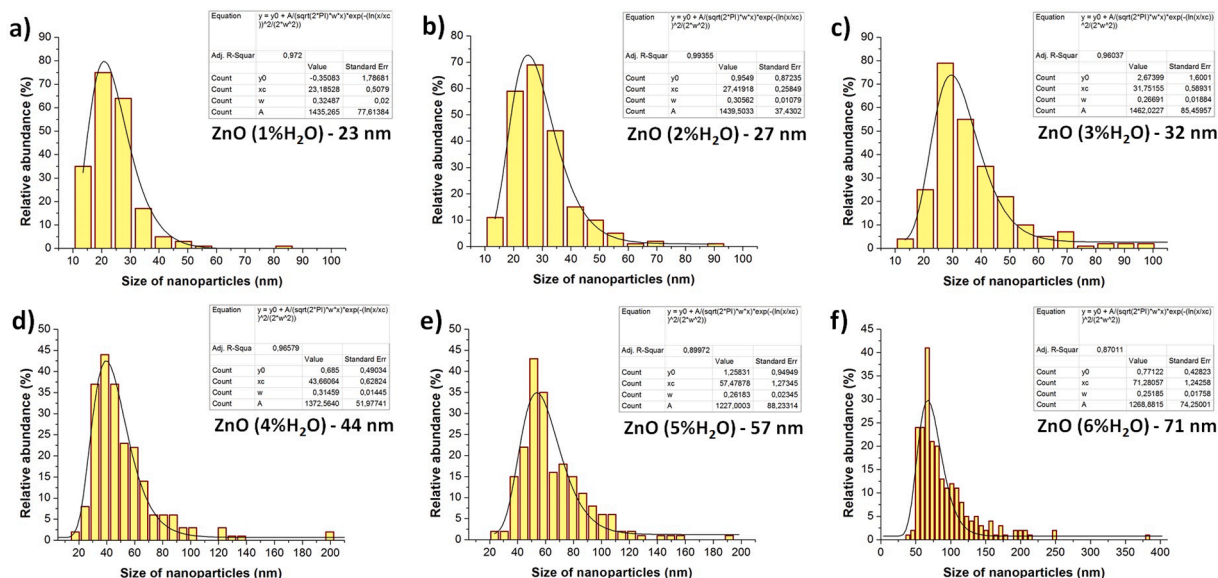


Fig. 7. The histogram of the particle size distribution of ZnO NPs (TEM method): a) 1% H<sub>2</sub>O, b) 2% H<sub>2</sub>O, c) 3% H<sub>2</sub>O, d) 4% H<sub>2</sub>O, (e) 5% H<sub>2</sub>O, f) 6% H<sub>2</sub>O.

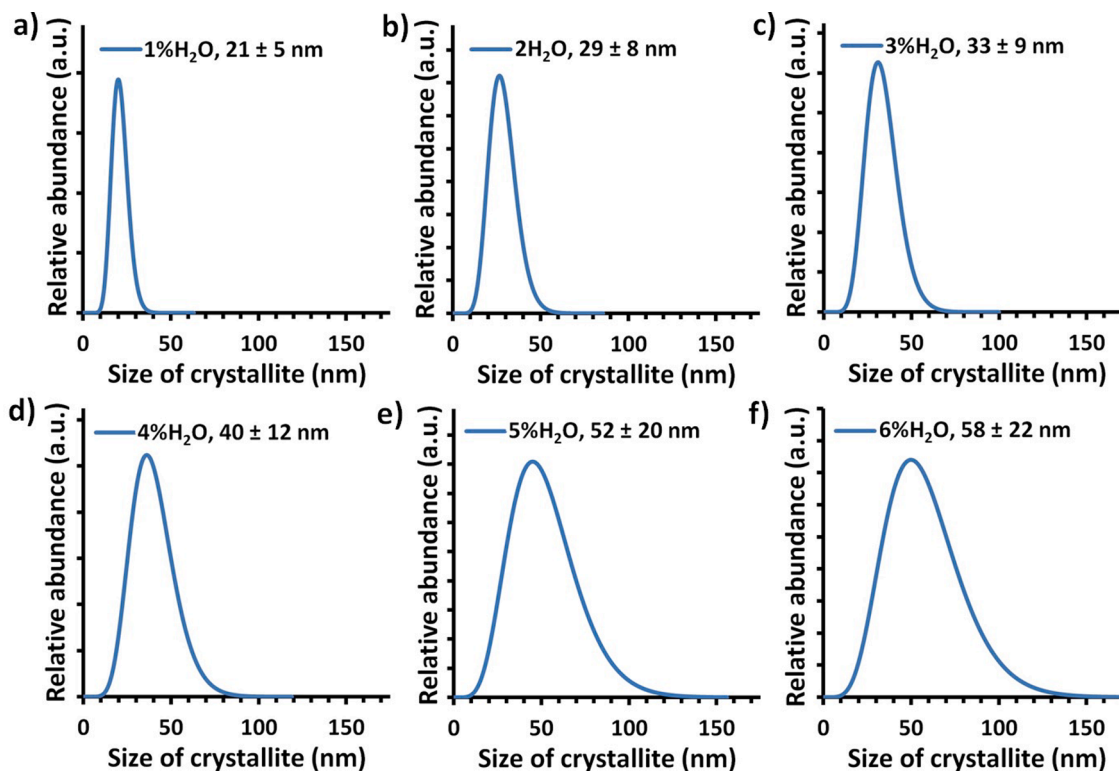


Fig. 8. Crystallite size distributions of ZnO NPs obtained using Nanopowder XRD Processor Demo, pre  $\alpha$  ver.0.0.8, © Pielaszek Research [83,84]: a) 1% H<sub>2</sub>O, b) 2% H<sub>2</sub>O, c) 3% H<sub>2</sub>O, d) 4% H<sub>2</sub>O, (e) 5% H<sub>2</sub>O, f) 6% H<sub>2</sub>O.

### 3.3. Density, specific surface area, average size and size distribution of ZnO NPs

The results of the analyses are presented in Tables 2 and 3 and Figs. 5–7. The theoretical density of ZnO is 5.606 g/cm<sup>3</sup> [86]. Generally, it is assumed that the closer the value of ZnO NPs sample density is to the value of the theoretical density of ZnO, the better the crystallinity of the obtained material. The increase in the H<sub>2</sub>O content from 1 wt% to 6 wt% in the solution of zinc acetate dissolved in ethylene glycol resulted in the increase in the density of ZnO NPs powder samples from 5.24 g/cm<sup>3</sup> to 5.51 g/cm<sup>3</sup> and the decrease in the specific surface area from 46.4 m<sup>2</sup>/g to 12.9 m<sup>2</sup>/g. In order to determine causes of the difference in density of ZnO NPs samples, TEM analyses were performed (Fig. 5). As shown in Fig. 5, ZnO NPs can be divided into two parts: internal crystalline core and external disorder shell. A decrease in thickness of the irregular disordered shell can be observed in the TEM images (Fig. 5), which explained the increase in the density of ZnO NPs in line with the increase in their size. Our earlier research on the change in stoichiometry of ZnO as a function of size change did not indicate significant differences [78], and therefore we believe that the disordered structures were an amorphous phase of ZnO. We reported a similar impact of the change in the water content on the density and specific surface area and at the same time on the size of the obtained ZnO NPs in publications [78,79,81]. The correlation between the density and specific surface area, in turn, is common knowledge [78,79,81,87–89].

The total pore volume value for the obtained ZnO NPs samples decreased from 0.2893 cm<sup>3</sup>/g to 0.1444 cm<sup>3</sup>/g in line with the decrease in their specific surface area (Table 1), which coincides with the literature [90,91]. The nitrogen adsorption isotherms in Fig. 6 indicate that the micropores are filled with nitrogen at very low pressures, then a monolayer is formed, subsequently successive layers, and the mesopores are filled. Close to the saturated vapour pressure  $p_0$ , the surface concentration of nitrogen rapidly increased because capillary condensation

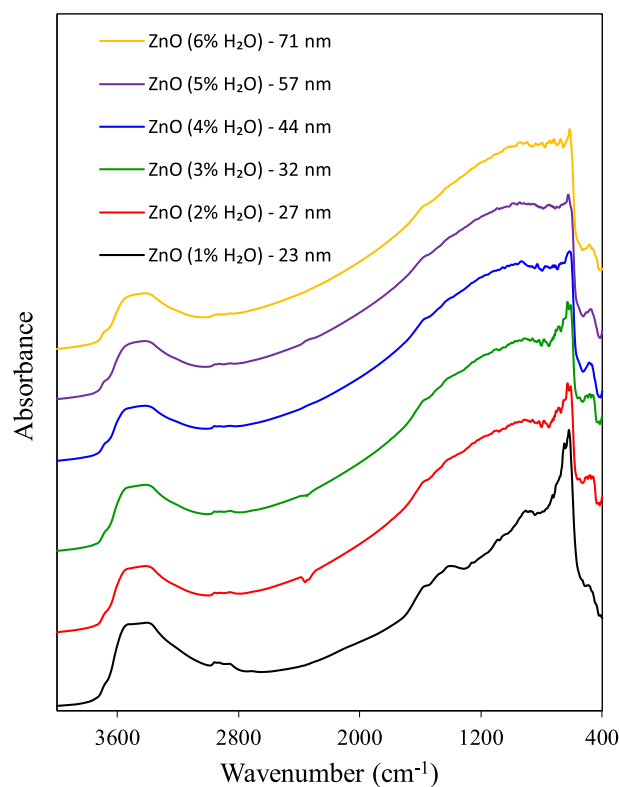


Fig. 9. FTIR/DR spectra for ZnO samples of various particle size.

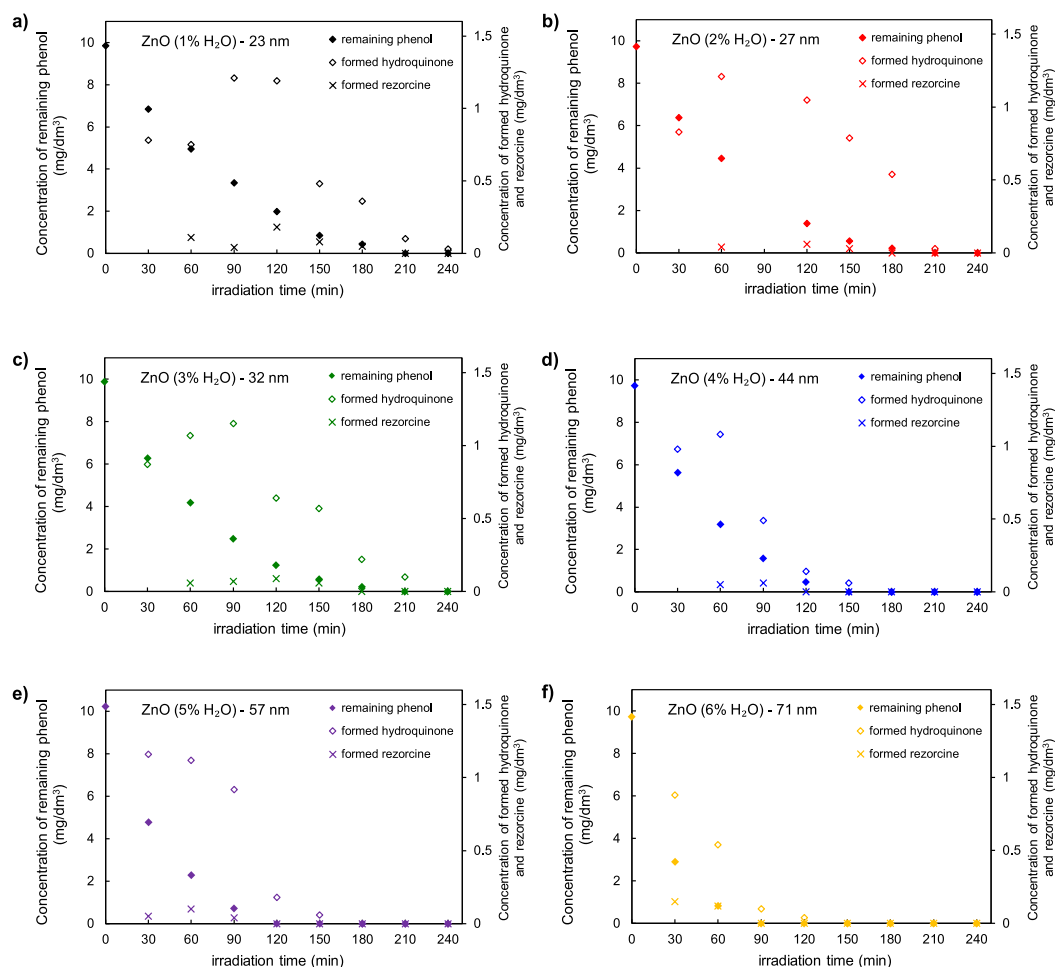


Fig. 10. Photocatalytic phenol decomposition on the tested ZnO samples under UV light irradiation.

occurred. The calculated average pore width (Table 2) is lower than 500 Å, which indicates that the obtained ZnO NPs samples displayed the mesoporous structure. An increase in the average pore width in line with the decrease in the specific surface area is observable in the case of samples from ZnO (1%H<sub>2</sub>O) to ZnO (5%H<sub>2</sub>O). The average pore width in ZnO (6%H<sub>2</sub>O) sample, in turn, is lower than in ZnO (5%H<sub>2</sub>O) sample, which is probably caused by the change in the shape of the obtained ZnO NPs (Fig. 3).

To determine the average size of ZnO NPs, the microscopic TEM method and the method of converting the results of the specific surface area and density were employed (Table 3, Fig. 7). Both methods yielded converging results of the increase in the average size of NPs arising from the increase in the water content from 1% to 6%. The XRD results allowed calculating the average crystallite size and the crystallite size distribution (Fig. 8). The results of the average size of NPs obtained by four methods for samples from ZnO (1% H<sub>2</sub>O) to ZnO (4% H<sub>2</sub>O) are virtually identical. However, the results for ZnO (5%H<sub>2</sub>O) samples are located on the extremes of the standard deviations of these methods. The results for the ZnO (6% H<sub>2</sub>O) sample, in turn, are outside the standard deviations of the employed methods. If the properties of the tested NPs satisfy the assumptions of the methods employed for calculating their average size, i.e. NPs are spherical or quasi-spherical, highly monodisperse and monocrystalline, the obtained results display nearly ideal convergence [92–94]. In the case of the ZnO (6% H<sub>2</sub>O) sample, we explain the lack of convergence of the results with the lack of uniformity of the NPs shape and the noticeable difference in the sizes of individual NPs, which can be seen in the SEM image (Fig. 3f). Based on a comparison of the obtained results of the average particle size with the

average crystallite size, it can be concluded that the ZnO NPs obtained in the microwave solvothermal synthesis is built of single crystals.

### 3.4. Surface characterisation

The characterisation of the surface of tested ZnO nanoparticles with various size was performed with the FTIR spectroscopy, and the results are shown in Fig. 9.

It can be generally stated that the intensity of the broad peak at 3700–2900 cm<sup>-1</sup>, attributed to –OH stretching vibrations of water [95], decreases with the increase of ZnO nanoparticles size. The broad peak with low intensity at 3688 cm<sup>-1</sup> can be assigned to stretching vibration modes of isolated hydroxyl groups. The peaks at 548 and 1027 cm<sup>-1</sup> correspond to Zn–O bonds [96,97]. The low-intensity peak at about 2945 cm<sup>-1</sup> can be attributed to the presence of –CH<sub>2</sub> groups, remaining from organic precursors applied to the synthesis of the samples. It is possible to observe that the intensity of this peak found for all studied samples decreases with the increase of water content used in the fabrication process.

### 3.5. Photocatalytic degradability of phenol

The results of the investigation of the photocatalytic decomposition of phenol as well as the formation of co-products under UV and visible light on ZnO samples of various particle size are shown in Fig. 10 a-f and 11 a-f, respectively. The UV-assisted photodegradation was more efficient in comparison to visible light photoactivity.

It can be generally concluded that the photocatalytic performance of

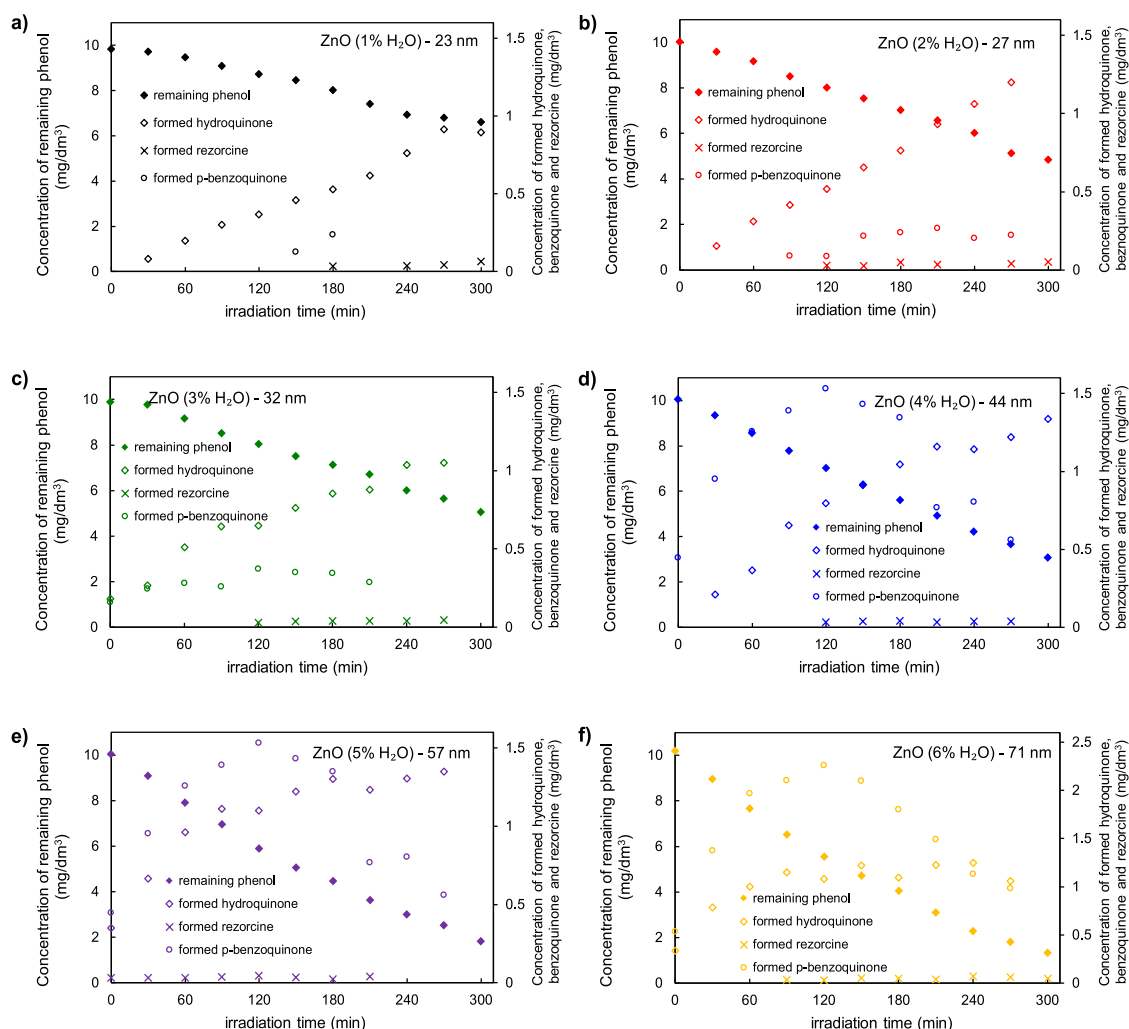


**Fig. 11.** Photocatalytic phenol decomposition on the tested ZnO samples under visible light irradiation.

ZnO nanoparticles strongly depends on particle size. As it can be seen in Figs. 10a-f and 11a-f, the photocatalytic activity enhances with the increase of the particle size of fabricated ZnO samples. In contrary to determining results, Jing et al. [98], as well as Pardeshi and Patil [75], confirmed typically known principle for nanoparticulate photoactive semiconductors that the reaction rate of photooxidation process increases with the decrease of the particle size, thus the increase of the specific surface area. These studies confirmed that the photocatalytic efficiency of ZnO nanoparticles increased with the increase of the particle size. The former assigned the photocatalytic activity to the surface properties (mainly specific surface area) of the ZnO ultrafine particles. The generated holes attack the surface hydroxyl and yield surface-bound hydroxyl radicals, while photoexcited electrons are captured by the surface oxygen deficiencies, restricting the recombination of these photogenerated charge carriers. This particular aspect has been verified based on intensity-modulated photocurrent/photovoltage measurements of the minority carriers' recombination time. The obtained results allow concluding that the charge carrier recombination rate of photo-generated holes decreases with the increase of the particle size. The results of the intensity-modulated photocurrent/photovoltage tests can be presented in the following order (starting from the photocatalyst with the slowest recombination time): ZnO (6% H<sub>2</sub>O)-71 nm < ZnO (5% H<sub>2</sub>O)-57 nm < ZnO (4% H<sub>2</sub>O)-44 nm, ZnO (3% H<sub>2</sub>O)-32 nm < ZnO (2% H<sub>2</sub>O)- 27 nm, ZnO (1% H<sub>2</sub>O)-23 nm.

Additionally, the hydroxyl groups, present on the surface of ZnO

nanoparticles, act as the centres for the photocatalytic reactions [98]. Yusoff et al. [99] found that the ZnO obtained under hydrothermal conditions was composed of agglomerates of zinc oxide nanoparticles with an average size of 71 nm. That agglomeration process may cause the reduction of the photocatalytic activity mainly due to the significant reduction of the surface area [100]. Interestingly, in our case, the highest decomposition rate of phenol was found for a sample with the average particle size of 71 nm (the largest particles of ZnO) and the lowest value of the specific surface area (12.9 m<sup>2</sup>/g). Moreover, based on a comparison of the obtained results of the average particle size with the average crystallite size, it can be concluded that the ZnO NPs obtained in the microwave solvothermal synthesis were not agglomerated. This is in line with results obtained by Li et al. [76]. Xu et al. [73] summarised that the preparation method of the nanoparticulate ZnO is commonly taken as the main factor that determined the photocatalytic performance of tested material.

The intermediates (hydroquinone and rezorcine) formed during the UV-assisted photocatalytic oxidation of phenol were also studied (see Fig. 12a-f). It can be concluded that the formation of primary or secondary hydroxylated products of phenol decomposition is mediated by the generation of reactive oxygen species, notably hydroxyl radicals [59]. Typically, the addition of •OH radicals in the photocatalytic process proceeds by an electrophilic addition reaction and different intermediates are produced depending on the position of the substituted group for the OH position on the benzene ring [101]. Both determined

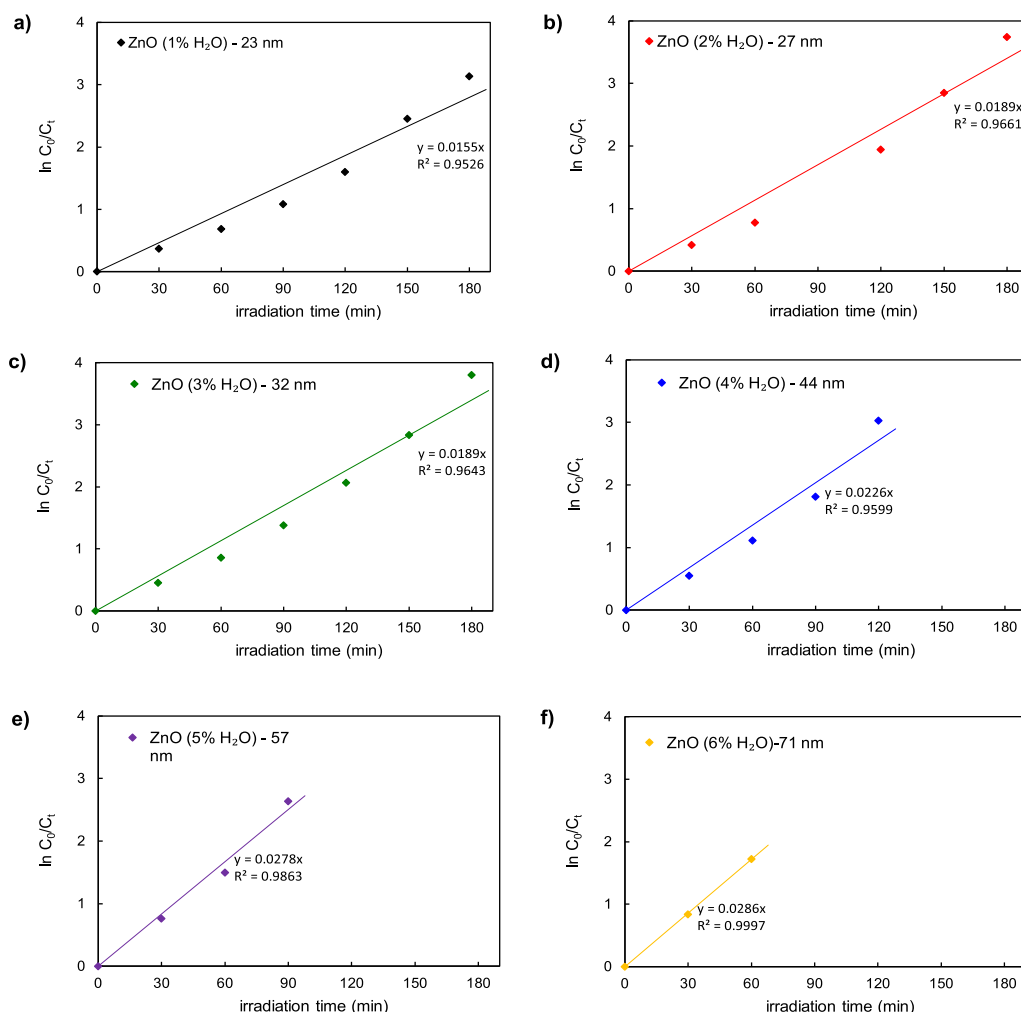


Fig. 12. Kinetic plots of phenol decomposition by ZnO photocatalysts under UV light irradiation.

by-products contained two hydroxyl groups substituted in a different position to the benzene ring (meta for rezorcine and para for hydroquinone). The formation of hydroxylated intermediates in the phenol photodegradation process confirms the role of  $\cdot\text{OH}$  radicals as reactive species what was also noticed by Dodd et al. [9].

In case of the visible light-assisted photodegradation of phenol it was confirmed that the process of degradation both main compound and its derivatives occurs slower, thus, less efficient. The presence of p-benzoquinone as a co-product was additionally noted.

The qualitative analysis of by-products formed during UV light irradiation allowed concluding that the concentration of both intermediates was rather low. However, the para-position in benzene ring was favourable to be substituted with hydroxyl groups to generate higher amounts of hydroquinone in reaction suspension. Additionally, for smaller ZnO nanoparticles (23–32 nm), hydroquinone and rezorcine by-products were firstly produced for 90 and 120 min, respectively, and after that time decomposed as the primary pollutant. For larger ZnO nanoparticles (44 and 57 nm) the decomposition of both intermediates started approx. after 60 min of UV radiation of phenol solution and the immediate degradation of by-products was observed for 71 nm-sized ZnO.

In the visible light-assisted photodegradation process the concentration of formed rezorcine was rather low for all tested samples. The amount of generated hydroquinone was generally higher in comparison to degradation of phenol under UV light, and it started being decomposed for 150 min only for 71 nm-sized ZnO sample. The para-position

in benzoquinone molecule was favourable to be substituted with OH groups to generate higher amounts of p-benzoquinone in comparison to hydroquinone for ZnO NPs with the size of 44, 57 and 71 nm. What is more, for these samples the latter-mentioned intermediate started being degraded after 120 min.

The kinetics of the phenol photooxidation was found to obey the Langmuir–Hinshelwood model. Figs. 12a-f and 13a-f present the kinetics is the pseudo-first-order concerning the phenol concentration under UV and Vis light irradiation, respectively. The apparent rate constant ( $k$ ) is proportional to the photocatalytic efficiency of the tested nanoparticles: the higher  $k$  value the higher efficiency of the photocatalytic oxidation reaction. Idris et al. [102] stated that a higher decomposition rate indicated more reactive oxygen species, and water molecules at the surface of the sample vigorously promoted the degradation of phenol.

The calculated results confirmed that the particle size had a decisive impact on the effectiveness of the photocatalytic oxidation of phenol. Fig. 14 presents the relation between average particle size and rate constant value listed for total phenol removal from reaction suspension. It can be clearly stated from Fig. 14a that the  $k_{UV}$  value was similar for ZnO NPs with 27 and 32 nm as well as 57 and 71 nm. No difference in total degradation time was noted for samples with 27 and 32 nm. However, in the case of larger nanoparticles, the total phenol degradation was 30 min faster for the sample with a larger particle size (71 nm). The influence of the ZnO particle size on the efficiency of photocatalytic degradation of phenol was also confirmed in case of visible light-assisted process. Despite the fact that the rate of phenol decomposition was much

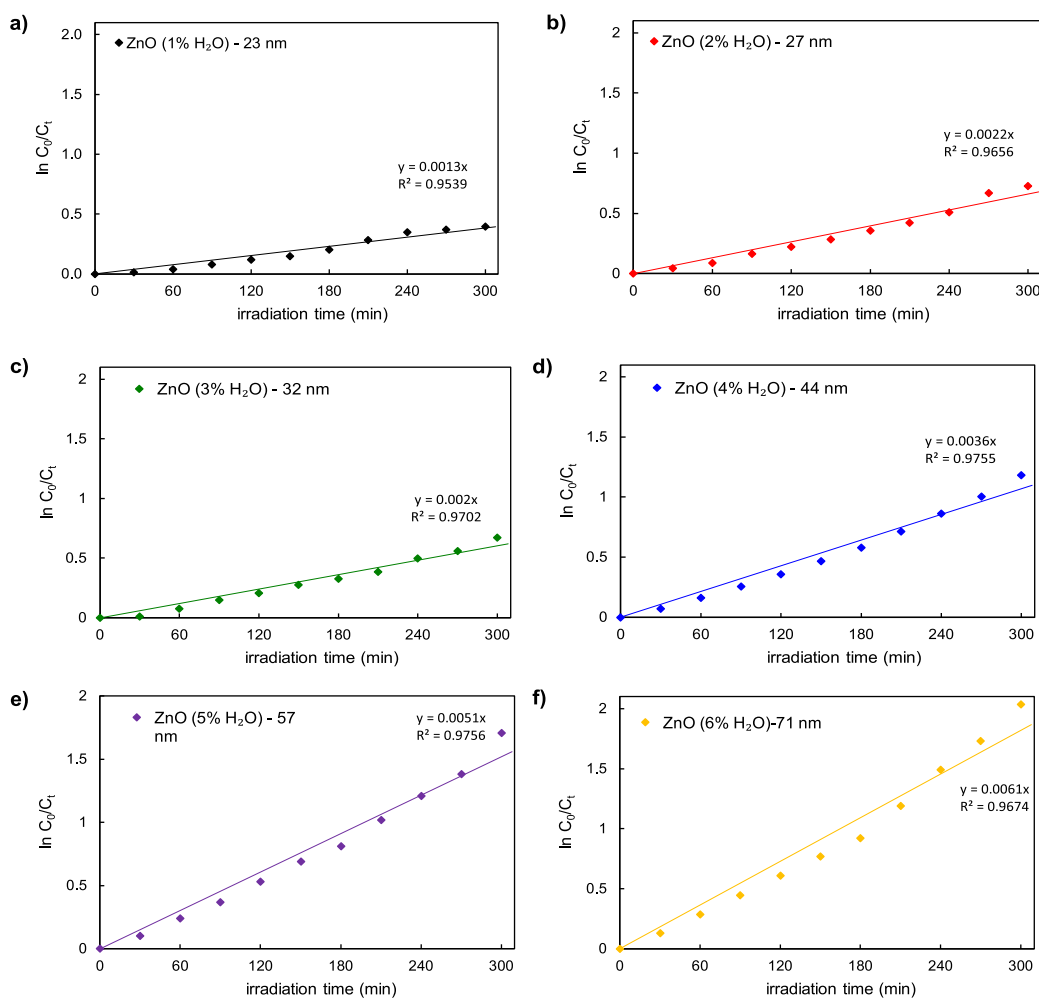


Fig. 13. Kinetic plots of phenol decomposition by ZnO photocatalysts under Vis light irradiation.

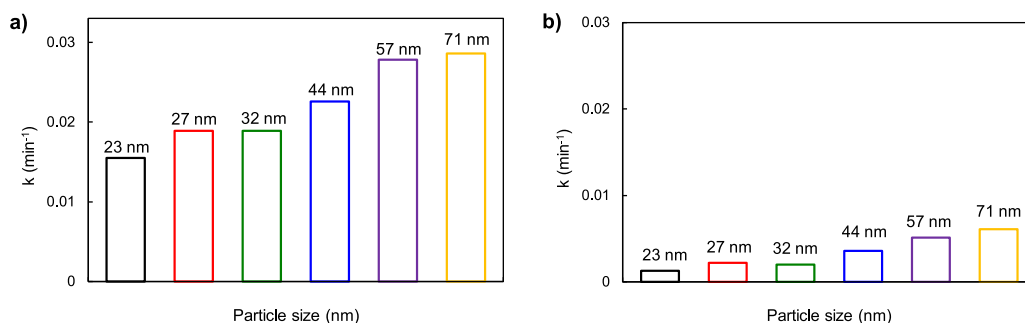


Fig. 14. Influence of the particle size of ZnO photocatalysts on the rate constant for total phenol degradation under: a) UV and b) visible light.

lower, the trend of  $k_{\text{Vis}}$  values was similar to  $k_{\text{UV}}$  – the apparent rate constant was approx. the same for ZnO NPs with the size of 27 and 32 nm, as well as 57 and 71 nm.

#### 4. Conclusions

The microwave solvothermal reaction permitted to obtain ZnO NPs with average size between 23 nm and 71 nm with uniform morphology and narrow size distribution. The photocatalytic performance of ZnO NPs increased with the increase of the particle size for both UV and Vis light irradiation. The highest reaction rate for phenol degradation was

found for ZnO sample with the average particle size of 71 nm (total degradation of phenol after 90 min of UV radiation). Low concentrations of rezorcline and hydroquinone (found as a degradation co-products of phenol degradation) were finally photooxidized after 90 and 150 min, respectively. The presence of p-benzoquinone as an additional intermediate product of phenol photodegradation under visible light was confirmed. Despite the fact that the efficiency of the Vis-assisted photodecomposition was significantly lower than the UV photooxidation, the trend of the obtained results was similar for both processes. The intensity-modulated photocurrent/photovoltage studies confirmed that the recombination time of the minority carriers (in this case positively

charged holes) was the longest for ZnO photocatalyst with the largest particles size. Hence, the increase of the photocatalytic activity with the NPs size in this experiment was attributable to the decrease in the charge carrier recombination rate.

### CRedit authorship contribution statement

**E. Kusiak-Nejman:** Conceptualization, Methodology, Investigation, Writing - original draft, Writing - review & editing. **J. Wojnarowicz:** Conceptualization, Methodology, Investigation, Writing - original draft, Writing - review & editing. **A.W. Morawski:** Formal analysis, Supervision. **U. Narkiewicz:** Writing - original draft, Supervision. **K. Sobczak:** Investigation, Writing - original draft, Writing - review & editing. **S. Gierlotka:** Investigation, Writing - original draft. **W. Lojkowski:** Investigation, Writing - original draft, Supervision.

### Declaration of Competing Interest

The authors declare that they have no known competing financial interests or personal relationships that could have appeared to influence the work reported in this paper.

### Acknowledgements

The paper was prepared as a result of the execution of “PRELUDIUM 10” research project, ref. No. UMO-2015/19/N/ST5/03668, financed by the National Science Centre, Poland.

A part of the research was carried out using equipment funded by the CePT project, reference: POIG.02.02.00-14-024/08, financed by the European Regional Development Fund within the Operational Programme “Innovative Economy” for 2007–2013.

The authors would also like to thank J. Mizeracki from the Institute of High Pressure Physics of the Polish Academy of Sciences.

### References

- [1] C. Burda, X. Chen, R. Narayanan, M.A. El-Sayed, Chemistry and properties of nanocrystals of different shapes, *Chem. Rev.* 105 (2005) 1025–1102. <https://pubs.acs.org/doi/10.1021/cr030063a>.
- [2] C.N.R. Rao, G.U. Kulkarni, P.J. Thomas, P.P. Edwards, Size-dependent chemistry: properties of nanocrystals, *Chemistry* 8 (2002) 28–35. [https://doi.org/10.1002/1521-3765\(20020104\)8:1<28::AID-CHEM28>3.0.CO;2-B](https://doi.org/10.1002/1521-3765(20020104)8:1<28::AID-CHEM28>3.0.CO;2-B).
- [3] S. Carrettin, P. Concepcion, A. Corma, J.M.L. Nieto, V.F. Puentes, Nanocrystalline CeO<sub>2</sub> increases the activity of Au for CO oxidation by two orders of magnitude, *Angew. Chem. Int. Ed.* 43 (2004) 2538–2540. <https://onlinelibrary.wiley.com/doi/full/10.1002/anie.200353570>.
- [4] L.H. Hu, Q. Peng, Y.D. Li, Selective synthesis of Co<sub>3</sub>O<sub>4</sub> nanocrystal with different shape and crystal plane effect on catalytic property for methane combustion, *J. Am. Chem. Soc.* 130 (2008) 16136–16137. <https://doi.org/10.1021/ja806400e>.
- [5] A.S. Crampton, M.D. Rotzer, C.J. Ridge, B. Yoon, F.F. Schweinberger, U. Landman, U. Heiz, Assessing the concept of structure sensitivity or insensitivity for sub-nanometer catalyst materials, *Surf. Sci.* 652 (2016) 7–19. <https://doi.org/10.1016/j.susc.2016.02.006>.
- [6] W. Tu, Y. Zhou, Z. Zou, Photocatalytic conversion of CO<sub>2</sub> into renewable hydrocarbon fuels: state-of-the-art accomplishment, challenges, and prospects, *Adv. Mater.* 26 (2014) 4607–4626. <https://doi.org/10.1002/adma.201400087>.
- [7] C.-C. Wang, Z. Zhang, J. Ying, Photocatalytic decomposition of halogenated organics over nanocrystalline titania, *Nanostr. Mater.* 9 (1997) 583–586. [https://doi.org/10.1016/S0965-9773\(97\)00130-X](https://doi.org/10.1016/S0965-9773(97)00130-X).
- [8] Z. Zhang, C.-C. Wang, R. Zakaria, J.J. Ying, Role of particle size in nanocrystalline TiO<sub>2</sub>-based photocatalysts, *J. Phys. Chem. B* 102 (1998) 10871–10878. <https://doi.org/10.1021/jp982948>.
- [9] A.C. Dodd, A.J. McKinley, M. Saunders, T. Tsuzuki, Effect of particle size on the photocatalytic activity of nanoparticulate zinc oxide, *J. Nanopart. Res.* 8 (2006) 43–51. <https://doi.org/10.1007/s11051-005-5131-z>.
- [10] N. Murakami, S. Kawakami, T. Tsubota, T. Ohno, Dependence of photocatalytic activity on the particle size of a shape controlled anatase titanium(IV) oxide nanocrystal, *J. Mol. Catal. A: Chem.* 358 (2012) 106–111. <https://doi.org/10.1016/j.molcata.2012.03.003>.
- [11] K. Koci, L. Obalova, L. Matejova, D. Placha, Z. Lacny, J. Jirkovsky, O. Solcova, Effect of TiO<sub>2</sub> particle size on the photocatalytic reduction of CO<sub>2</sub>, *Appl. Catal. B: Environm.* 89 (2009) 494–502. <https://doi.org/10.1016/j.apcatb.2009.01.010>.
- [12] E. Kusiak-Nejman, A. Wanag, L. Kowalczyk, J. Kapica-Kozar, Ch. Colbeau-Justin, M.G. Méndez-Medrano, A.W. Morawski, Graphene-oxide TiO<sub>2</sub> and reduced graphene oxide-TiO<sub>2</sub> nanocomposites: insight in charge-carrier lifetime measurements, *Catal. Today* 287 (2017) 189–195. <https://doi.org/10.1016/j.cattod.2016.11.008>.
- [13] A. Zielinska-Jurek, E. Kowalska, J.W. Sobczak, W. Lisowski, B. Ohtani, A. Zaleska, Preparation and characterisation of monometallic (Au) and bimetallic (Ag/Au) modified-titania photocatalysts activated by visible light, *Appl. Catal. B Environ.* 101 (2011) 504–514. <https://doi.org/10.1016/j.apcatb.2010.10.022>.
- [14] J. Lee, S. Mubeen, X. Ji, G.D. Stucky, Plasmonic photoanodes for solar water splitting with visible light, *Nano Lett.* 12 (9) (2012) 5014–5019. <https://doi.org/10.1021/nl302796f>.
- [15] K. Du, G. Liu, X. Chen, K. Wang, Charge separation and photocurrent enhancement on black TiO<sub>2</sub> nanotubes co-sensitized with Au nanoparticles and PbS quantum dots, *Electrochim. Acta* 277 (2018) 244–254. <https://doi.org/10.1016/j.electacta.2018.05.014>.
- [16] D. Dolat, S. Mozia, R.J. Wrobel, D. Moszynski, B. Ohtani, N. Guskos, A.W. Morawski, Nitrogen-doped, metal modified rutile titanium dioxide as photocatalysts for water remediation, *Appl. Catal. B: Environ.* 162 (2015) 310–318. <https://doi.org/10.1016/j.apcatb.2014.07.001>.
- [17] N. Yazdanpour, S. Sharifnia, Photocatalytic conversion of greenhouse gases (CO<sub>2</sub> and CH<sub>4</sub>) using copper phthalocyanine-modified TiO<sub>2</sub>, *Solar Energy Mater. Sol. Cells* 118 (2013) 1–8. <https://doi.org/10.1016/j.solmat.2013.07.051>.
- [18] R. Ameta, S. Benjamin, A. Ameta, S.C. Ameta, Photocatalytic degradation of organic pollutants: a review, *Mater. Sci. Forum* 734 (2013) 247–272. <https://doi.org/10.4028/www.scientific.net/MSF.734.247>.
- [19] P. Singh, A. Ojha, A. Borthakur, S. Rishikesh, D. Lahiry, D. Tiwary, P.K. Mishra, Emerging trends in photodegradation of petrochemical wastes: a review, *Environ. Sci. Pollut. Res.* 23 (2016) 22340–22364. <https://doi.org/10.1007/s11356-016-7373-y>.
- [20] P. Singh, A. Borthakur, A review on biodegradation and photocatalytic degradation of organic pollutants: a bibliometric and comparative analysis, *J. Clean. Prod.* 196 (2018) 1669–1680. <https://doi.org/10.1016/j.jclepro.2018.05.289>.
- [21] P.V.L. Reddy, K.H. Kim, B. Kavitha, V. Kumar, N. Raza, S. Kalagara, Photocatalytic degradation of bisphenol A in aqueous media: a review, *J. Environ. Manag.* 213 (2018) 189–205. <https://doi.org/10.1016/j.jenvman.2018.02.059>.
- [22] M. Pelaez, N.T. Nolan, S.C. Pillai, M.K. Seery, P. Falaras, A.G. Kontos, P.S. M. Dunlop, J.W.J. Hamilton, J.A. Byrne, K. O’Shea, M.H. Entezari, D. Dionysiou, A review on the visible light active titanium dioxide photocatalysts for environmental applications, *Appl. Catal. B Environ.* 125 (2012) 331–349. <https://doi.org/10.1016/j.apcatb.2012.05.036>.
- [23] L. Cheng, Q. Xiang, Y. Liao, H. Zhang, CdS-Based photocatalysts, *Energy Environ. Sci.* 11 (2018) 1362–1391. <https://doi.org/10.1039/C7EE03640J>.
- [24] C.B. Ong, L.Y. Ng, A.W. Mohammad, A review of ZnO nanoparticles as solar photocatalysts: synthesis, mechanisms and applications, *Renew. Sust. Energ. Rev.* 81 (2018) 536–551. <https://doi.org/10.1016/j.rser.2017.08.020>.
- [25] S.B.A. Hamid, S.J. Teh, C.W. Lai, Photocatalytic water oxidation on ZnO: a review, *Catalysts* 7 (2017) 93. <https://doi.org/10.3390/catal7030093>.
- [26] I.V. Tudose, M. Sucheai, ZnO for photocatalytic air purification applications, *IOP Conf. Ser.: Mater. Sci. Eng.* 133 (2016) 012040.
- [27] U. Ozgur, D. Hofstetter, H. Morkoc, ZnO devices and applications: a review of current status and future prospects, *Proc. IEEE* 98 (2010) 1255–1268. <https://doi.org/10.1109/JPROC.2010.2044550>.
- [28] C. Dette, M.A. Pérez-Osorio, C.S. Kley, P. Punke, C.E. Patrick, P. Jacobson, F. Giustino, S.J. Jung, K. Kern, TiO<sub>2</sub> anatase with a bandgap in the visible region, *Nano Lett.* 14 (2014) 6533–6538. <https://doi.org/10.1021/nl503131s>.
- [29] A. Kolodziejczak-Radzimska, T. Jesionowski, Zinc oxide—from synthesis to application: a review, *Materials* 7 (2014) 2833–2881. <https://doi.org/10.3390/ma7042833>.
- [30] A. Ali, A.R. Phull, M. Zia, Elemental zinc to zinc nanoparticles: Is ZnO NPs crucial for life? Synthesis, toxicological and environmental concerns, *Nanotechnol. Rev.* 7 (2018) 413–441. <https://doi.org/10.1515/ntrev-2018-0067>.
- [31] A. Król, P. Pomastowski, K. Rafińska, V. Railean-Plugaru, B. Buszewski, Zinc oxide nanoparticles: synthesis, antisepsis activity and toxicity mechanism, *Adv. Colloid Interface Sci.* 249 (2017) 37–52. <https://doi.org/10.1016/j.cis.2017.07.033>.
- [32] Suresh C. Pillai, John M. Kelly, Raghavendra Rameshc, Declan E. McCormack, Advances in the synthesis of ZnO nanomaterials for varistor devices, *J. Mater. Chem. C* 1 (2013) 3268–3281. <https://doi.org/10.1039/C3TC00575E>.
- [33] Shakeel Ahmed, Annu, Saif AliChaudhry, Saiqa Ikrama, A review on biogenic synthesis of ZnO nanoparticles using plant extracts and microbes: a prospect towards green chemistry, *J. Photochem. Photobiol., B* 166 (2017) 272–284. <https://doi.org/10.1016/j.jphotobiol.2016.12.011>.
- [34] K. Żelechowska, Methods of ZnO nanoparticles synthesis, *BioTechnologia* 95 (2014) 150–159. <https://doi.org/10.5114/bta.2014.48857>.
- [35] Marina Bandeira, Marcelo Giovanela, Mariana Roesch-Ely, Declan M. Devine, Janainada Silva Crespo, Green synthesis of zinc oxide nanoparticles: a review of the synthesis methodology and mechanism of formation, *Sustain. Chem. Pharmacy* 15 (2020) 100223.
- [36] A. Singh, N.B. Singh, S. Afzal, et al., Zinc oxide nanoparticles: a review of their biological synthesis, antimicrobial activity, uptake, translocation and biotransformation in plants, *J. Mater. Sci.* 53 (2018) 185–201. <https://doi.org/10.1007/s10853-017-1544-1>.
- [37] Happy Agarwal, S. Venkat Kumar, S. Rajeshkumar, A review on green synthesis of zinc oxide nanoparticles – an eco-friendly approach, *Resource-Efficient Technologies* 3 (2017) 406–413. <https://doi.org/10.1016/j.refit.2017.03.002>.
- [38] M.A. Borysiewicz, ZnO as a functional material, a review, *Crystals* 9 (2019) 505. <https://doi.org/10.3390/cryst9100505>.
- [39] X. Xue, Z. Zhou, B. Peng, M.M. Zhu, Y.J. Zhang, W. Ren, Z.G. Ye, X. Chen, M. Liu, Review on nanomaterials synthesized by vapor transport method: growth and

- their related applications, RSC Adv. 5 (2015) 79249–79263, <https://doi.org/10.1039/C5RA13349A>.
- [40] J. Wojnarowicz, T. Chudoba, W. Lojkowski, A review of microwave synthesis of zinc oxide nanomaterials: reactants, process parameters and morphologies, *Nanomaterials* 10 (2020) 1086, <https://doi.org/10.3390/nano10061086>.
- [41] E. Mohammadi, M. Aliofkhaezai, M. Hasanpoor, M. Chipara, Hierarchical and complex ZnO nanostructures by microwave-assisted synthesis: morphologies, growth mechanism and classification, *Crit. Rev. Solid State Mater. Sci.* 43 (43) (2018) 475–541, <https://doi.org/10.1080/10408436.2017.1397501>.
- [42] A. McLaren, T. Valdes-Solis, G. Li, S. Chi Tsang, Shape and size effects of ZnO nanocrystals on photocatalytic activity, *J. Am. Chem. Soc.* 131 (2009) 12540–12541, <https://doi.org/10.1021/ja9052703>.
- [43] Y. Sun, L. Chen, Y. Bao, Y. Zhang, J. Wang, M. Fu, J. Wu, D. Ye, The applications of morphology controlled ZnO in catalysis, *Catalysts* 6 (2016) 188, <https://doi.org/10.3390/catal6120188>.
- [44] A. Majcher, J. Wijek, J. Przybylski, T. Chudoba, J. Wojnarowicz, A novel reactor for microwave hydrothermal scale-up nanopowder synthesis, *Int. J. Chem. React. Eng.* 11 (2013) 361–368, <https://doi.org/10.1515/ijcre-2012-0009>.
- [45] S. Dąbrowska, T. Chudoba, J. Wojnarowicz, W. Lojkowski, Current trends in the development of microwave reactors for the synthesis of nanomaterials in laboratories and industries: a review, *Crystals* 8 (2018) 379, <https://doi.org/10.3390/cryst8100379>.
- [46] G. Yashni, A. Al-Gheethi, R. Mohamed, Md. Sohrab Hossain, Amani Filzah Kamil, Vikneswara Abirama Shanmugan, *Water Environ. J.* (2020), <https://doi.org/10.1111/wej.12619>.
- [47] A. Balcha, O.P. Yadav, T. Dey, Photocatalytic degradation of methylene blue dye by zinc oxide nanoparticles obtained from precipitation and sol-gel methods, *Environ. Sci. Pollut. Res.* 23 (2016) 25485–25493, <https://doi.org/10.1007/s11356-016-7750-6>.
- [48] A.A. Yaqoob, N.H. Mohd Noor, A. Serrà, M.N. Mohamad Ibrahim, Advances and challenges in developing efficient graphene oxide-based ZnO photocatalysts for dye photo-oxidation. *Nanomaterials* 10 (2020), 932. <https://doi.org/10.3390/nano10050932>.
- [49] N. Roy, S. Chakraborty, ZnO as photocatalyst: an approach to waste water treatment, *Mater. Today: Proc.* (2020), <https://doi.org/10.1016/j.matpr.2020.06.264>.
- [50] T. Varadavenkatesan, E. Lyubchik, S. Pai, A. Pugazhendhi, R. Vinayagam, R. Selvaraj, Photocatalytic degradation of Rhodamine B by zinc oxide nanoparticles synthesized using the leaf extract of *Cyanometra ramiflora*, *J. Photochem. Photobiol., B* 199 (2019) 111621, <https://doi.org/10.1016/j.jphotobiol.2019.111621>.
- [51] X. Chen, Z. Wu, D. Liu, Preparation of ZnO photocatalyst for the efficient and rapid photocatalytic degradation of azo dyes, *Nanoscale Res. Lett.* 12 (2017) 143, <https://doi.org/10.1186/s11671-017-1904-4>.
- [52] Q. Zhang, M. Xu, B. You, Q. Zhang, H. Yuan, K.K. Ostrikov, Oxygen vacancy-mediated ZnO nanoparticle photocatalyst for degradation of methylene blue, *Appl. Sci.* 8 (2018) 353, <https://doi.org/10.3390/app8030353>.
- [53] G.E. Lau, C.A. Che Abdullah, W.A.N. Wan Ahmad, S. Assaw, A.L.T. Zheng, Eco-friendly photocatalysts for degradation of dyes, *Catalysts* 10 (2020) 1129, <https://doi.org/10.3390/catal10101129>.
- [54] P. Franco, O. Sacco, I. De Marco, V. Vaiano, Zinc oxide nanoparticles obtained by supercritical antisolvent precipitation for the photocatalytic degradation of crystal violet dye, *Catalysts* 9 (2019) 346, <https://doi.org/10.3390/catal9040346>.
- [55] J. Al-Sabahi, T. Bora, M. Al-Abri, J. Dutta, Controlled defects of zinc oxide nanorods for efficient visible light photocatalytic degradation of phenol, *Materials* 9 (4) (2016) 238, <https://doi.org/10.3390/ma9040238>.
- [56] B. Dong, X. Yu, Z. Dong, et al., Facile synthesis of ZnO nanoparticles for the photocatalytic degradation of methylene blue, *J. Sol-Gel Sci. Technol.* 82 (2017) 167–176, <https://doi.org/10.1007/s10971-016-4297-4>.
- [57] C. Wang, D. Wu, P. Wang, Y. Ao, J. Hou, J. Qian, Effect of oxygen vacancy on enhanced photocatalytic activity of reduced ZnO nanorod arrays, *Appl. Surf. Sci.* 325 (15) (2015) 112–116, <https://doi.org/10.1016/j.apsusc.2014.11.003>.
- [58] S. Chatterjee, A. Kumar Kar, Oxygen-Vacancy-Dependent Photocatalysis for the Degradation of MB Dye Using UV Light and Observation of Förster Resonance Energy Transfer (FRET) in PANI-Capped ZnO, *J. Phys. Chem. C* 124 (2020), 18284–18301. <https://doi.org/10.1021/acs.jpcc.0c03248>.
- [59] M. Choquette-Labbé, W.A. Shewa, J.A. Lalman, S.R. Shanmugan, Photocatalytic degradation of phenol and phenol derivatives using a nano-TiO<sub>2</sub> catalyst: integrating quantitative and qualitative factors using response surface methodology, *Water* 6 (2014) 1785–1806. <https://doi.org/10.3390/w6061785>.
- [60] S.P. DeviPriya, S. Yesodharan, Photocatalytic degradation of phenol in water using TiO<sub>2</sub> and ZnO, *J. Environ. Biol.* 31 (2010) 247–249.
- [61] H. Benhebal, M. Chaib, T. Salmon, J. Geens, A. Leonard, S.D. Lambert, M. Crine, B. Heinrichs, Photocatalytic degradation of phenol and benzoic acid using zinc oxide powders prepared by the sol-gel process, *Alexandria Eng. J.* 52 (2013) 517–523. <https://doi.org/10.1016/j.aej.2013.04.005>.
- [62] N.A. Yusoff, S.A. Onga, L.N. Hob, Y.S. Wong, W.F. Khalik, Degradation of phenol through solar-photocatalytic treatment by zinc oxide in aqueous solution, *Desalination Water Treat.* 57 (2016) 1621–1628. <https://doi.org/10.1080/19443994.2014.908414>.
- [63] D.J. Naghan, A. Azari, N. Mirzaei, A. Velayati, F.A. Tapouk, S. Adabi, M. Pirsahab, K. Sharafi, Parameters effecting on photocatalytic degradation of the phenol from aqueous solutions in the presence of ZnO nanocatalyst under irradiation of UV-C light, *Bulg. Chem. Commun.* 47 (2015) 14–18.
- [64] S. Saeedi, H. Godini, M. Almasian, G. Shams-Khorramabadi, B. Kamarehie, P. Mostafaie, F. Taheri, Photocatalytic degradation of phenol in water solutions using ZnO nanoparticles immobilized on glass, *J. Adv. Environ. Health Res.* 3 (2015) 204–213. <https://doi.org/10.22102/jaehr.2015.40204>.
- [65] D. Rajamanickam, M. Shanthi, Photocatalytic degradation of an organic pollutant by zinc oxide – solar process, *Arab. J. Chem.* 9 (2016) 1858–1868. <https://doi.org/10.1016/j.arabj.2012.05.006>.
- [66] N. Yusoff, L.N. Ho, S.A. Ong, Y.S. Wong, W. Khalik, M.F. Ridwan, Enhanced photodegradation of phenol by ZnO nanoparticles synthesised through sol-gel method, *Sains Malaysiana* 46 (2017) 2507–2514. <https://doi.org/10.17576/jsm-2017-4612-28>.
- [67] H. Dewidar, S.A. Nosier, A.H. El-Shazly, Photocatalytic degradation of phenol solution using Zinc Oxide/UV, *J. Chem. Health Saf.* 25 (2018) 2–11. <https://doi.org/10.1016/j.jchhas.2017.06.001>.
- [68] I. Prabha, S. Lathasree, Photodegradation of phenol by zinc oxide, titania and zinc oxide–titania composites: nanoparticle synthesis, characterisation and comparative photocatalytic efficiency, *Mat. Sci. Semicon. Proc.* 26 (2014) 603–613. <https://doi.org/10.1016/j.mssp.2014.05.031>.
- [69] Y. Tao, Z.L. Cheng, K.E. Ting, X.J. Yin, Photocatalytic degradation of phenol using a nanocatalyst: the mechanism and kinetics, *J. Catal.* 2013 (2013) 364275. <https://doi.org/10.1155/2013/364275>.
- [70] N. Morales-Flores, U. Pal, E. Sánchez Mora, Photocatalytic behavior of ZnO and Pt-incorporated ZnO nanoparticles in phenol degradation, *Appl. Catal. A-Gen.* 394 (2011) 269–275.
- [71] I. Udom, P.D. Myers, M.K. Ram, A.F. Hepp, E. Archibong, E.K. Stefanakos, D. Y. Goswami, Optimisation of photocatalytic degradation of phenol using simple photocatalytic reactor, *Am. J. Anal. Chem.* 5 (2014) 743–750. <https://doi.org/10.4236/ajac.2014.511083>.
- [72] J. Ye, X. Li, J. Hong, J. Chen, Q. Fan, Photocatalytic degradation of phenol over ZnO nanosheets immobilised on montmorillonite, *Mat. Sci. Semicon. Proc.* 39 (2015) 17–22. <https://doi.org/10.1016/j.mssp.2015.04.039>.
- [73] X. Xu, Z. Yi, D. Chen, X. Duan, Z. Zhou, X. Fan, M. Jiang, Evaluation of photocatalytic production of active oxygen and decomposition of phenol in ZnO suspensions, *Rare Met.* 30 (2011) 188–191. <https://doi.org/10.1007/s12598-011-0266-9>.
- [74] N. Xu, Z. Shi, Y. Fan, J. Dong, J. Shi, M.Z.C. Hu, Effects of particle size of TiO<sub>2</sub> on photocatalytic degradation of methylene blue in aqueous suspensions, *Ind. Eng. Chem. Res.* 38 (1999) 373–379. <https://doi.org/10.1021/ie980378u>.
- [75] S.K. Pardeshi, A.B. Patil, Effect of morphology and crystallite size on solar photocatalytic activity of zinc oxide synthesised by solution free mechanochemical method, *J. Mol. Catal. A-Chem.* 308 (2009) 32–40. <https://doi.org/10.1016/j.molcata.2009.03.023>.
- [76] D. Li, H. Haneda, Morphologies of zinc oxide particles and their effects on photocatalysis, *Chemosphere* 51 (2003) 129–137. [https://doi.org/10.1016/S0045-6535\(02\)00787-7](https://doi.org/10.1016/S0045-6535(02)00787-7).
- [77] K.M. Parida, S. Parija, Photocatalytic degradation of phenol under solar radiation using microwave irradiated zinc oxide, *Sol. Energy* 80 (2006) 1048–1054. <https://doi.org/10.1016/j.solener.2005.04.025>.
- [78] J. Wojnarowicz, A. Opalinska, T. Chudoba, S. Gierlotka, R. Mukhovskiy, E. Pietrzykowska, K. Sobczak, W. Lojkowski, Effect of water content in ethylene glycol solvent on the size of ZnO nanoparticles prepared using microwave solvothermal synthesis, *J. Nanomater.* 2016 (2016) 2789871. <https://doi.org/10.1155/2016/2789871>.
- [79] J. Wojnarowicz, T. Chudoba, I. Koltsov, S. Gierlotka, S. Dworakowska, W. Lojkowski, Size control mechanism of ZnO nanoparticles obtained in microwave solvothermal synthesis, *Nanotechnology* 29 (2018) 065601. <https://doi.org/10.1088/1361-6528/aa00ef>.
- [80] J. Wojnarowicz, T. Chudoba, S. Gierlotka, W. Lojkowski, Effect of microwave radiation power on the size of aggregates of ZnO NPs prepared using microwave solvothermal synthesis, *Nanomaterials* 8 (2018) 343. <https://doi.org/10.3390/nano8050343>.
- [81] J. Wojnarowicz, T. Chudoba, S. Gierlotka, K. Sobczak, W. Lojkowski, Size control of cobalt-doped ZnO nanoparticles obtained in microwave solvothermal synthesis, *Crystals* 8 (2018) 179. <https://doi.org/10.3390/cryst8040179>.
- [82] R. Pielaszek, FW15/45M method for determination of the grain size distribution from powder diffraction line profile, *J. Alloy. Compd.* 37 (2004) 128–132. <https://doi.org/10.1016/j.jallcom.2004.05.040>.
- [83] Nanopowder XRD Processor Demo, pre- $\alpha$ -ver.0.0.8, © Pielaszek Research. Available online: <http://science24.com/xrd/> (accessed on October 1 2018).
- [84] FW15/45M Method of evaluation of grain size distribution by powder diffraction. Available online: <http://science24.com/fw145m/> (accessed on October 1 2018).
- [85] A. Ashrafi, C. Jagadish, Review of zincblende ZnO: stability of metastable ZnO phases, *J. Appl. Phys.* 102 (2007) 071101. <https://doi.org/10.1063/1.2787957>.
- [86] M. Hjiri, L.E. Mir, S.G. Leonardi, Synthesis, characterization and sensing properties of azo and izaro nanomaterials, *Chemosensors* 2 (2014) 121–130. <https://doi.org/10.3390/chemosensors2020121>.
- [87] A. Opalinska, I. Malka, W. Dzwolak, T. Chudoba, A. Presz, W. Lojkowski, Size-dependent density of zirconia nanoparticles, *Beilstein J. Nanotechnol.* 6 (6) (2015) 27–35. <https://doi.org/10.3762/bjnano.6.4>.
- [88] S. Kusnieruk, J. Wojnarowicz, A. Chodara, T. Chudoba, S. Gierlotka, W. Lojkowski, Influence of hydrothermal synthesis parameters on the properties of hydroxyapatite nanoparticles, *Beilstein J. Nanotechnol.* 7 (2016) 1586–1601. <https://doi.org/10.3762/bjnano.7.153>.
- [89] D. Smoleń, T. Chudoba, S. Gierlotka, A. Kedzierska, W. Lojkowski, K. Sobczak, W. Świączkowski, K.J. Kurzydłowski, Hydroxyapatite nanopowder synthesis with

- a programmed resorption rate, *J. Nanomater.* 2012 (2012) 841971. <https://doi.org/10.1155/2012/841971>.
- [90] M.A. Ismail, K.K. Taha, A. Modwi, L. Khezami, ZnO nanoparticles: surface and X-ray profile analysis, *J. Ovonic. Res.* 14 (2018) 381–393.
- [91] S.K. Lee, A.Y. Kim, J.Y. Lee, S.H. Ko, S.W. Kim, Facile Synthesis of ZnO nanoparticles and their photocatalytic activity, *Bull. Korean Chem. Soc.* 35 (2014) 7. <https://doi.org/10.5012/bkcs.2014.35.7.2004>.
- [92] H. Borchert, E.V. Shevchenko, A. Robert, I. Mekis, A. Kornowski, G. Grübel, H. Weller, Determination of nanocrystal sizes: a comparison of TEM, SAXS, and XRD studies of highly monodisperse CoPt<sub>3</sub> particles, *Langmuir* 21 (2005) 1931–1936. <https://doi.org/10.1021/la0477183>.
- [93] S. Pabisch, B. Feichtenschlager, G. Kickelbick, H. Peterlik, Effect of interparticle interactions on size determination of zirconia and silica based systems – a comparison of SAXS, DLS, BET, XRD and TEM, *Chem. Phys. Lett.* 521 (2012) 91–97. <https://doi.org/10.1016/j.cplett.2011.11.049>.
- [94] S. Myhra, J.C. Rivière, *Characterisation of Nanostructures*, first ed., CRC Press, Taylor & Francis Group, Boca Raton, FL, USA, 2013, ISBN 9781138198630.
- [95] T. Chankhanittha, S. Nanan, Hydrothermal synthesis, characterisation and enhanced photocatalytic performance of ZnO toward degradation of organic azo dye, *Mater. Lett.* 226 (2018) 79–82. <https://doi.org/10.1016/j.matlet.2018.05.032>.
- [96] S. Kakarndee, S. Nanan, SDS capped and PVA capped ZnO nanostructures with high photocatalytic performance toward photodegradation of reactive red (RR141) azo dye, *Environ. Chem. Eng.* 6 (2018) 74–94. <https://doi.org/10.1016/j.jece.2017.11.066>.
- [97] H. Kumar, R. Rani, Structural and optical characterisation of ZnO nanoparticles synthesised by microemulsion route, *Int. Lett. Chem. Phys. Astron.* 14 (2013) 26–36. <https://doi.org/10.18052/www.scipress.com/ILCPA.19.26>.
- [98] L. Jing, Z. Xu, X. Sun, J. Shang, W. Cai, The surface properties and photocatalytic activities of ZnO ultrafine particles, *Appl. Surf. Sci.* 180 (2001) 308–314. [https://doi.org/10.1016/S0169-4332\(01\)00365-8](https://doi.org/10.1016/S0169-4332(01)00365-8).
- [99] N.A. Yusoff, L.N. Ho, S.A. Ong, Y.S. Wong, W.F. Khalik, Photocatalytic activity of zinc oxide (ZnO) synthesised through different methods, *Desalin. Water Treat.* 57 (2015) 12496–12507. <https://doi.org/10.1080/19443994.2015.1054312>.
- [100] Z.H. Liu, Y. Kanjo, S. Mizutani, Removal mechanisms for endocrine disrupting compounds (EDCs) in wastewater treatment-physical means, biodegradation, and chemical advanced oxidation: A review, *Sci. Total Environ.* 407 (2009) 731–748. <https://doi.org/10.1016/j.scitotenv.2008.08.039>.
- [101] D.S. Bhatkhande, V.G. Pangarkar, A. Beenackers, Photocatalytic degradation for environmental applications - a review, *J. Chem. Technol. Biotechnol.* 77 (2001) 102–116.
- [102] A. Idris, N. Hassan, R. Rashid, A.F. Ngomsik, Kinetics and regeneration studies of photocatalytic magnetic separable beads for chromium(VI) reduction under sunlight, *J. Hazard. Mater.* 186 (2010) 629–635.